Quantitative and Repetitive Control of Subcellular Protein–Protein Interaction Using a Photochromic Dimerizer

Takato Mashita,[1,#] Toshiyuki Kowada,[1,2,3,#] Hayashi Yamamoto,[4] Satoshi Hamaguchi,[3] Toshitaka Matsui,[1,2,3] and Shin Mizukami[1,2,3,*]

[1] Graduate School of Science, Tohoku University, 6-3, Aoba, Aramaki, Aoba-ku, Sendai, Miyagi 980–8578, Japan

[2] Institute of Multidisciplinary Research for Advanced Materials, Tohoku University, 2-1-1, Katahira, Aoba-ku, Sendai, Miyagi 980–8577, Japan

[3] Graduate School of Life Sciences, Tohoku University, 2-1-1, Katahira, Aoba-ku, Sendai, Miyagi 980–8577, Japan

[4] Institute for Advanced Medical Sciences, Nippon Medical School, 1-1-5, Sendagi, Bunkyo-ku, Tokyo 113-8602, Japan

[#] These authors contributed equally to this work.

* E-mail: shin.mizukami@tohoku.ac.jp

Abstract

Artificial control of intracellular protein dynamics with high precision provides deep insight into complicated biomolecular networks. Optogenetics and caged compound-based chemically induced dimerization (CID) systems are emerging as tools for spatiotemporally regulating intracellular protein dynamics. However, both technologies face several challenges for accurate control such as the duration of activation, deactivation rate, and repetition cycles. Herein, we report a photochromic CID system that employs the photoisomerization of a ligand so that both association and dissociation are controlled by light, enabling quick, repetitive, and quantitative regulation of the target protein localization upon violet and green light illumination. We also demonstrated the usability of the photochromic CID system as a potential tool to finely manipulate intracellular protein dynamics to study diverse cellular processes. Utilizing this system to manipulate PINK1/Parkin-mediated mitophagy, we showed that PINK1 recruitment to the mitochondria can promote Parkin recruitment to proceed with mitophagy.

Cellular events are spatiotemporally regulated by the dynamics of various biomolecules, such as protein-protein interactions or protein translocation[1,2]. The artificial regulation of these dynamics with precision in time and space offers valuable insights into the causality between biomolecular dynamics and cellular processes[3,4]. Chemical and optogenetic tools have been reported to be versatile methods that provide exquisite control of biomolecular dynamics[5]. Optogenetic tools employ photoresponsive proteins whose conformations change upon illumination[6–10]. Most optogenetic tools are activated by blue light and are deactivated when the light input is stopped. This property has allowed reversible induction of light-dependent protein association or dimerization, achieving light-dependent regulation of diverse cellular processes within a few seconds. These tools enable the dynamic control of signaling pathways, such as the Ras/Erk pathway[11,12] and the stromal-interaction-molecule-1-mediated signaling pathway[13], and elucidate complex signaling networks. However, because CRY2/CIBN exhibits thermal deactivation after stopping illumination[7,14], continuous light exposure, which may cause photodamage, is required to maintain the activated state. In addition, the slow turn-off rate could result in the loss of high temporal control. Hence, as implemented by PhyB/PIF[6], light-triggered bidirectional regulation has several advantages over the blue light-activation optogenetic system. However, even though the PhyB/PIF system allows excellent spatiotemporal control, it also faces other problems, such as the large size of the protein modules (99 and 11 kDa) and the bimodal absorption spectra overlapping with the excitation/emission of various fluorescent proteins[15,16], which limit their widespread use in the control of biomolecules.

Another tool for regulating cellular processes is chemically induced dimerization (CID) systems furnished by chemical dimerizers, which involve two ligand moieties to induce dimerization or association of target proteins[17,18]. CID systems are suitable for investigating long-term cellular events such as mitosis[19] by sustaining protein dimers. Recently, photoactivatable[20–23] or photocleavable[24,25] CID systems, termed caged CID, have been reported and have attracted attention as new chemical tools for regulating intracellular protein dynamics. Caged CID systems provide a higher spatiotemporal precision than conventional CID systems. We

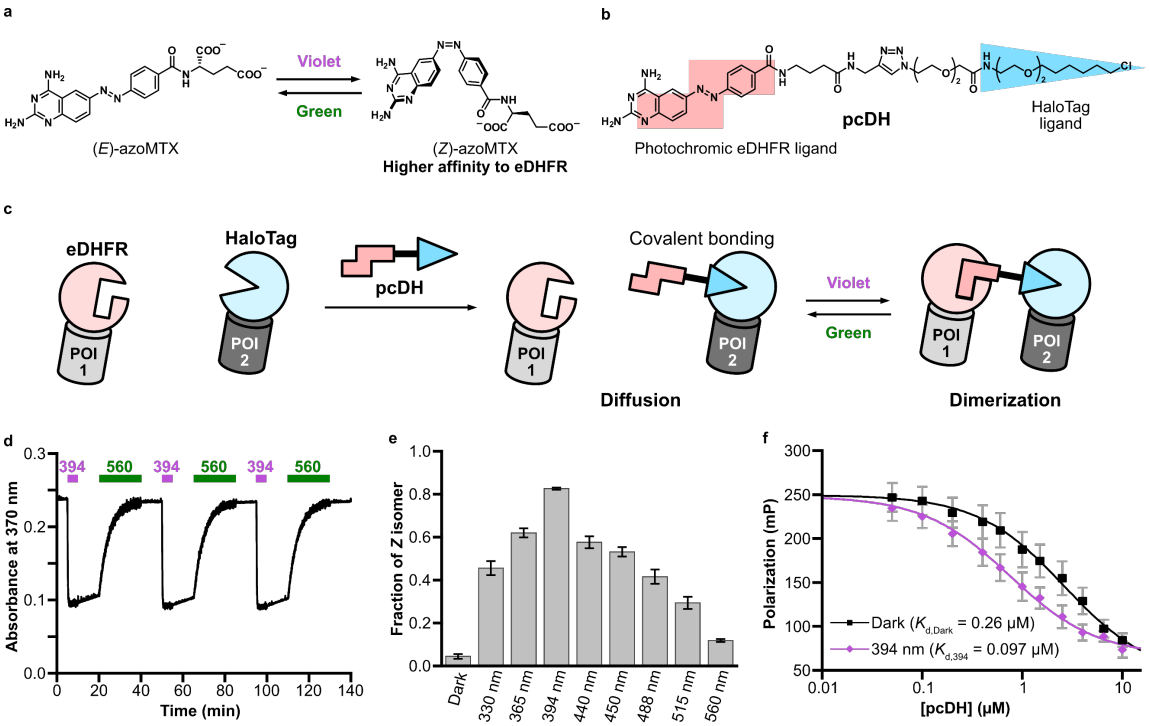

Fig. 1 | Design and characterization of pcDH. a, The structure and photoisomerization of azoMTX. The *Z* isomer has higher affinity to eDHFR than the *E* isomer. **b**, Chemical structure of the photochromic dimerizer, pcDH. **c**, Schematic illustration of the photochromic CID system. A HaloTag ligand forms covalent bond with HaloTag protein, and a photochromic eDHFR ligand binds to eDHFR in a photoreversible manner as shown in Fig. 1a. **d**, Time course of absorption changes at 370 nm under alternating light irradiation (394/10 nm and 560/10 nm). Light intensity was set to 5.0 mW cm^{-2} for each wavelength. **e**, Fractions of *Z* isomer of pcDH at the various photostationary states, determined by HPLC analyses. Data shown are mean ± s.d. (n = 3). **f**, Competitive binding assay of pcDH and eDHFR using fluorescence polarization. pcDH under 394-nm was irradiated with violet light (394/10 nm, 5.0 mW cm^{-2}) for 5 min before the measurement. R^2 value was >0.99. Data shown are mean ± s.d. (n = 4).

also developed a caged covalent-CID system that maintains stable protein dimers applicable to gel electrophoresis[26]. These caged CID systems revealed complex cellular systems, such as the specialized properties of a kinesin motor[27] and the molecular mechanisms of spindle asymmetry[28]. Furthermore, using two different caging groups in a chemical dimerizer, bidirectional photocontrol of protein localization and diffusion has been achieved in a single cycle[29,30]. However, caged CID systems, in principle, cannot be repetitively switched on and off, unlike optogenetic tools.

In this study, we developed a 'photochromic CID' system, which allows repetitive protein dimerization and dissociation by light. The photochromic CID system consists of two protein tags and a dimerizer tethering a covalent ligand for one tag and a photochromic ligand for the other tag. Photoreversible protein dimerization is achieved by photoisomerization of the photochromic ligand, enabling protein translocation to various subcellular compartments. This system allowed bidirectional control of protein association and diffusion by dual-wavelength light irradiation and achieved fast and durable localization of the target proteins. Furthermore, the translocation level of the target protein was varied by the irradiation light wavelength or the combination of dual-wavelength light with different intensities. Finally, this system was applied for the optical induction of mitophagy by regulating the subcellular localization of PINK1.

Results

Design and characterization of photochromic dimerizer. We previously developed a photoreversible inhibitor for *E. coli* dihydrofolate reductase (eDHFR, 18 kDa), azoMTX (Fig. 1a)[31], identical to phototrexate, a photoactivated chemotherapy agent targeting human DHFR developed by Matera et al.[32]. Violet light irradiation, typically at 394 nm, isomerizes azoMTX from the *E* isomer to the *Z* isomer, whereas green light, typically at 560 nm, induces reverse isomerization from *Z* to *E*. Since (*Z*)-azoMTX has a higher affinity to eDHFR than the *E* isomer, azoMTX was associated with and dissociated from eDHFR repeatedly by alternating irradiation with different wavelengths of light. Accordingly, we designed a small-molecule dimerizer pcDH (Fig. 1b), which involves both an azoMTX-based photochromic eDHFR ligand and HaloTag ligand, to establish

a photochromic CID system. One of the carboxy groups of azoMTX was removed for the design of pcDH to enhance its cell membrane permeability. Since the HaloTag ligand, a chloroalkyl group, specifically forms a covalent bond with a HaloTag protein (33 kDa)[33], pcDH is spontaneously labeled with HaloTag-fused proteins in living cells. Under dark conditions, binding to eDHFR can be suppressed because the thermally stable *E* form of the photochromic ligand shows a low affinity to eDHFR. UV to violet light irradiation isomerizes the photochromic ligand and enhances the affinity to eDHFR to induce HaloTag–eDHFR dimerization. Subsequently, green light irradiation inversely isomerizes the photochromic ligand from *Z* to *E* and reduces its affinity to eDHFR, leading to dissociation of the protein dimer (Fig. 1c).

pcDH was synthesized according to Supplementary Scheme 1, and its photophysical properties were studied in an aqueous solution. pcDH exhibited photochromism upon illumination at various wavelengths (Supplementary Fig. 1), and repetitive photoisomerization was achieved by alternating light at 394 and 560 nm (Fig. 1d). The *E* and *Z* isomer fractions

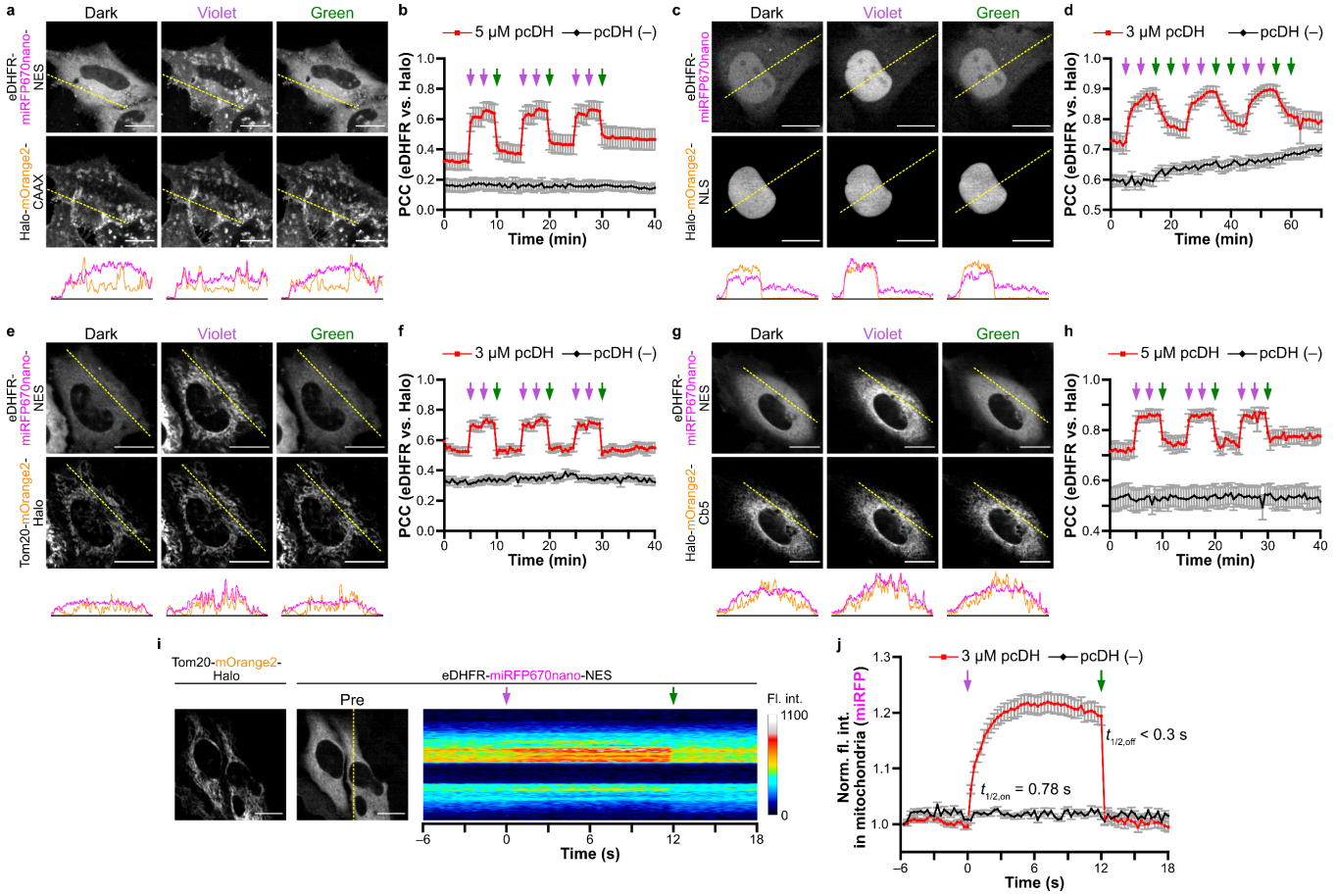

Fig. 2 | Photoreversible translocation of cytosolic proteins to various subcellular compartments. a,**b**, Photochromism-induced recruitment of cytosolic proteins to the plasma membrane. Confocal fluorescence images of HeLa cells expressing Halo-mOrange2-CAAX and eDHFR-miRFP670nano-NES before and after light illumination at 405 nm (violet) and 555 nm (green) (**a**). Time-course changes of Pearson's correlation coefficient (PCC) (**b**). **c**,**d**, Photochromism-induced recruitment of cytosolic proteins to the nucleus. Confocal fluorescence images of HeLa cells expressing Halo-mOrange2-NLS and eDHFR-miRFP670nano before and after light illumination at 405 nm (violet) and 555 nm (green) (**c**). Time-course changes of PCC (**d**). **e**,**f**, Photochromism-induced recruitment of cytosolic proteins to the MOM. Confocal fluorescence images of HeLa cells expressing Tom20-mOrange2-Halo and eDHFR-miRFP670nano-NES before and after light illumination at 405 nm (violet) and 555 nm (green) (**e**). Time-course changes of PCC (**f**). **g**,**h**, Photochromism-induced recruitment of cytosolic proteins to the ER. Confocal fluorescence images of HeLa cells expressing Halo-mOrange2-Cb5 and eDHFR-miRFP670nano-NES before and after light illumination at 405 nm (violet) and 555 nm (green) (**g**). Time-course changes of PCC (**h**). **i**,**j**, Translocation rate evaluation of eDHFR-miRFP670nano-NES between the cytosol and the MOM. Mitochondrial localization of Tom20-mOrange2-Halo is shown on the left (**i**). The kymograph was generated along a yellow dashed line (**i**). Time-course changes of fluorescence intensity in the mitochondria. The $t_{1/2,on}$ (0.78 ± 0.40 s) was determined using a mono-exponential function (**j**). The line profiles indicate the fluorescence intensity of mOrange2 (orange) and miRFP670nano (magenta), measured along the yellow lines in the images. The arrows indicate light irradiation of 405 nm (violet) and 555 nm (green), respectively. Data shown are mean ± s.e.m., *n* = 13–15 cells (**b**,**d**,**f**,**h**) or 38 cells (for **i**,**j**), three independent experiments. Scale bars, 20 μm.

in the photostationary states were varied according to the irradiation wavelength (*Z* isomer at 394 nm: 82.6 ± 0.5%, *Z* isomer at 560 nm: 11.6 ± 0.8%; mean ± s.d., $n = 3$) (Fig. 1e, Supplementary Fig. 2). The dissociation constant (K_d) between eDHFR and pcDH was determined by a competitive binding assay using an eDHFR-selective inhibitor, trimethoprim (TMP)[34], conjugated with fluorescein (TMP-Fl) (Supplementary Scheme 2). The results of the affinity assay ($K_{d,Dark} = 0.26 \pm 0.04$ μM, $K_{d,394} = 0.097 \pm 0.015$ μM, mean ± s.d. ($n = 4$); Fig. 1f, Supplementary Fig. 3) indicated that pcDH under 394-nm irradiation had an approximately three times higher affinity to eDHFR than under dark condition. Although the difference between $K_{d,Dark}$ and $K_{d,394}$ was smaller than that of azoMTX[31], which is likely due to the modification of the photochromic ligand moiety to provide cell membrane permeability, this result indicated that pcDH can be used as a photoreversible protein dimerizer.

Photoreversible protein translocation. Next, we attempted to control subcellular protein translocation by using pcDH. HeLa cells were transfected with two plasmids encoding eDHFR-fused miRFP670nano with a nuclear export signal (NES) sequence (eDHFR-miRFP670nano-NES) and HaloTag-fused mOrange2 with a CAAX sequence (Halo-mOrange2-CAAX), targeting the cytosolic interface of the plasma membrane. After the cells were incubated with 5 μM pcDH for 1 h, fluorescence images were acquired by excitation at 640 nm for miRFP670nano and 555 nm for mOrange2 using a spinning-disk confocal laser microscope. eDHFR-miRFP670nano-NES was initially spread in the cytosol (Fig. 2a, Dark). When the cells were irradiated with violet light (405 nm), the eDHFR-miRFP670nano-NES quickly translocated to the plasma membrane, where Halo-mOrange2-CAAX was expressed (Fig. 2a, Violet). Subsequently, green light (555 nm) irradiation promptly caused the eDHFR-miRFP670nano-NES to diffuse back into the cytosol (Fig. 2a, Green). This translocation of eDHFR-miRFP670nano-NES between the cytosol and plasma membrane was reversible and repeatable (Fig. 2b, Supplementary Video 1). The translocation was almost completed with low-intensity and instantaneous irradiation (60 μW, 100 ms). This was confirmed by the result that the second irradiation 2.5 min after the first irradiation induced only a small increase (less than 0.1) in the Pearson's correlation coefficient (PCC) value. In the absence of pcDH, no translocation of eDHFR-miRFP670nano-NES was observed upon either violet or green light illumination (Supplementary Fig. 4). Moreover, the addition of excess TMP suppressed the translocation of eDHFR-miRFP670nano-NES to the plasma membrane upon violet light illumination (Extended Data Fig. 1, Supplementary Video 2). These results indicate that photoreversible translocation is due to the photochromism-based affinity change of pcDH with eDHFR.

To validate the versatility of this photochromic CID system, we assessed the photoreversible protein translocation to various intracellular compartments. Halo-mOrange2-NLS, Halo-mOrange2-Cb5 (Cb5: amino acids 100–134 of cytochrome *b*5), and Tom20-mOrange2-Halo were used to target the nucleus, endoplasmic reticulum (ER), and mitochondrial outer membrane (MOM), respectively. In every case, photoreversible protein translocation was observed (Fig. 2c–h, Supplementary Videos 3–5), as was the case with the plasma membrane. eDHFR-miRFP670nano-NES promptly translocated to the ER or mitochondria and diffused back into the cytosol upon light illumination (Fig. 2f,h). However, the translocation of eDHFR-miRFP670nano to and from the nucleus required a longer time (Fig. 2d). This delay is presumably because some barriers, such as nuclear pores, suppress the protein diffusion.

We further investigated the kinetics of protein translocation between the cytosol and the MOM. The higher time-resolution imaging analysis revealed the rapid recruitment to the MOM with 0.78 ± 0.40 s of the half-association time $t_{1/2,on}$ (mean ± s.d., $n = 38$ cells) upon violet light (405 nm) irradiation (Fig. 2i,j, Supplementary Fig. 5, Supplementary Video 6). On the other hand, the half-dissociation time $t_{1/2,off}$ upon green light (555 nm) irradiation was less than 0.3 s, which could not be precisely determined by the limitation of the measurement interval (300 ms) (Fig. 2i,j). To our knowledge, the association and dissociation rates of the photochromic CID system are faster than or comparable to those of other optogenetic tools (Supplementary Table 1)[6,35,36].

Quantitative regulation of subcellular protein recruitment. Because the proportion of *E* and *Z* isomers of pcDH at the photostationary state is dependent on the exposure light wavelength (Fig. 1e), we assumed that it would be possible to recruit the protein quantitatively based on light wavelength. HeLa cells transiently expressing eDHFR-miRFP670nano-NES and Halo-mOrange2-CAAX were treated with 5 μM pcDH, then irradiated with violet, blue, and green light. After blue light (445 nm) illumination, the fluorescence signals of HaloTag- and eDHFR-fused proteins were less colocalized than those after violet light illumination (Fig. 3a, Supplementary Video 7). The PCC representing the

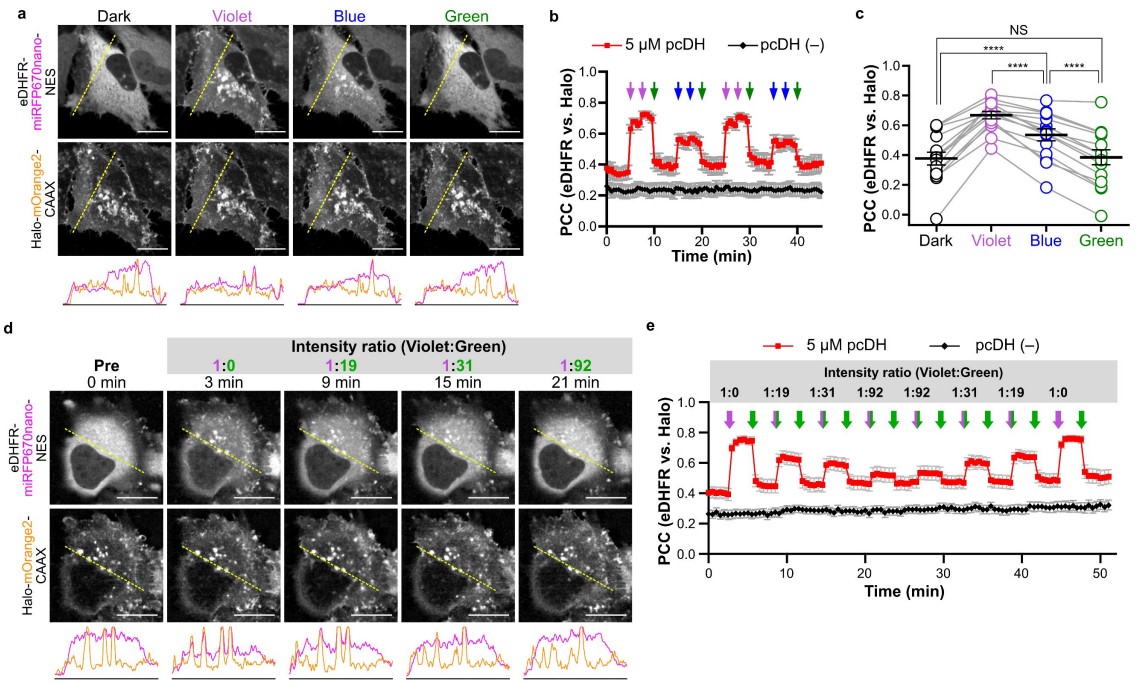

Fig. 3 | Quantitative recruitment of cytosolic proteins using the photochromic CID system. a, Wavelength-dependent recruitment of cytosolic proteins to the plasma membrane. Confocal fluorescence images of HeLa cells expressing Halo-mOrange2-CAAX and eDHFR-miRFP670nano-NES before (dark) and after light illumination at 405 nm (violet), 445 nm (blue), and 555 nm (green). The line profiles indicate the fluorescence intensity of mOrange2 (orange) and miRFP670nano (magenta), measured along the yellow lines in the images. **b**, Time-course changes of PCC calculated from the imaging dataset of Fig. 3a. The arrows indicate light irradiation of 405 nm (violet), 445 nm (blue), and 555 nm (green), respectively. Data shown are mean ± s.e.m. **c**, Quantification of eDHFR recruitment upon light illumination. Data shown are mean ± s.e.m., Two-tailed paired Student's *t*-test. ****$P < 0.0001$ and not significant (NS) for $P > 0.05$. $n = 15$ cells, three independent experiments. **d**, Dual-wavelength-dependent recruitment of cytosolic proteins to the plasma membrane. Confocal fluorescence images of HeLa cells expressing Halo-mOrange2-CAAX and eDHFR-miRFP670nano-NES before (Pre) and after simultaneous illumination of violet (382.5–394.5 nm) and green (543–557.5 nm) lights with different intensity ratios (1:0, 1:19, 1:31, or 1:92). The line profiles indicate the fluorescence intensity of mOrange2 (orange) and miRFP670nano (magenta), measured along the yellow lines in the images. **e**, Time-course changes of PCC upon varying intensity ratio of violet and green lights. The two-colored arrows indicate simultaneous irradiation of violet and green light with described ratios on the arrows, and the violet and green arrows indicate violet and green light irradiation, respectively. Data shown are mean ± s.e.m. $n = 15$ cells (5 μM pcDH) or 20 cells (pcDH (−)), four independent experiments. Scale bar, 20 μm.

colocalization of eDHFR with HaloTag after the blue light illumination (PCC = 0.54 ± 0.04; mean ± s.e.m., $n = 15$ cells) was lower than that after violet light illumination (PCC = 0.67 ± 0.03) and higher than that after green light illumination (PCC = 0.38 ± 0.05) (Fig. 3b,c). A similar variation on the protein recruitment was also induced by treating different concentrations of TMP-HTL (Extended Data Fig. 2), which is a conventional chemical dimerizer for eDHFR and HaloTag (Supplementary Scheme 3). However, it is difficult to validate repetitively and quantitatively in the identical cells by the conventional CID system, unlikely by our photochromic CID.

We also examined the quantitative recruitment of the eDHFR-fused protein by simultaneous illumination with violet (382.5–394.5 nm) and green (543–557.5 nm) light with different intensity ratios (Supplementary Fig. 6). HeLa cells transiently expressing eDHFR-miRFP670nano-NES and Halo-mOrange2-CAAX were treated with pcDH, and time-lapse fluorescence images were acquired (Fig. 3d). The PCC value, which indicates the localization of eDHFR-miRFP670nano-NES to the plasma membrane, was the highest under violet light illumination and gradually decreased as the intensity of mixed green light increased, approaching the value when only green light was applied (Fig. 3e). This indicates that the *E*/*Z* isomer ratio of pcDH can be quantitatively adjusted by controlling the ratio of light intensity at the two wavelengths, resulting in fine recruitment of intracellular proteins in a photoreversible manner. This is one of the advantages of this system, which is based on fast photoreversible switching.

Optical manipulation of subcellular signal transduction to induce mitophagy. Finally, we applied the photochromic CID system for the optical manipulation of biomolecular networks in live cells. The autophagy-mediated degradation of mitochondria, termed mitophagy, is an essential intracellular

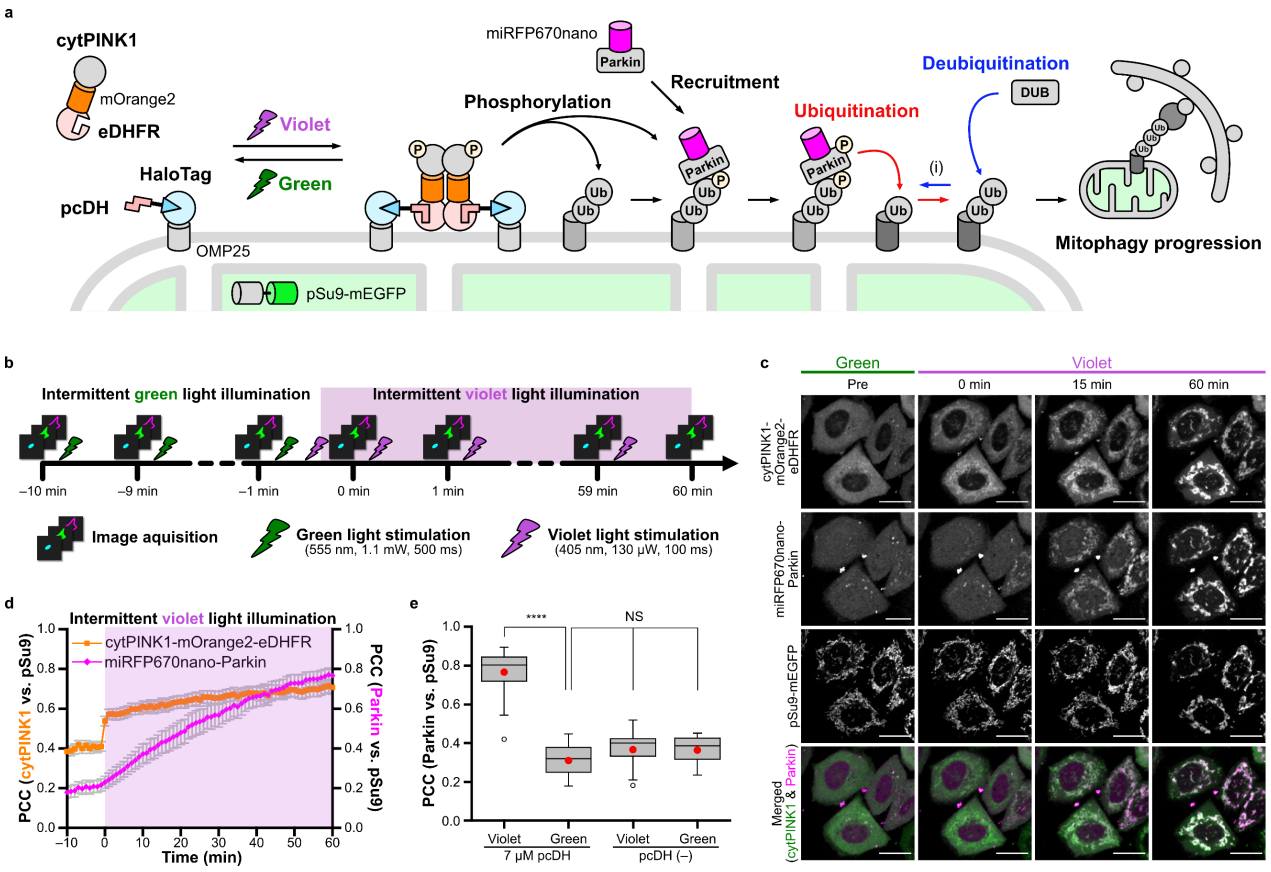

Fig. 4 | Optical regulation of mitophagy by the photochromic CID system. a, Schematic illustration of optical regulation of mitophagy induction using the photochromic CID system. DUB: Deubiquitinating enzyme. **b**, Illustration of intermittent light illumination (every 1 min) to retain localization of cytPINK1-mOrange2-eDHFR on the MOM. **c**,**d**, Violet-light-dependent recruitment of cytPINK1-mOrange2-eDHFR to the MOM followed by miRFP670nano-Parkin accumulation. Confocal fluorescence images of HeLa cells expressing cytPINK1-mOrange2-eDHFR, miRFP670nano-Parkin, pSu9-mEGFP, and Halo-OMP25. Violet light (405 nm) was illuminated before the image acquisition (0 min) and after every image acquisition (0–60 min). Scale bar, 20 μm (**c**). Time-dependent mitochondrial recruitment of cytPINK1-mOrange2-eDHFR and miRFP670nano-Parkin. The mean values (± s.e.m) of the PCC with the MOM (pSu9-mEGFP) were plotted (**d**). **e**, Quantification of Parkin localization on the MOM at 60 min. Red dots represent the mean values. Plots are constructed from the datasets in Fig. 4 and Extended Data Figs. 3 and 4. Two-tailed Welch's *t*-test. ****$P < 0.0001$ and not significant (NS) for $P > 0.05$. $n = 15$ cells, three independent experiments.

event for maintaining cellular homeostasis, in which damaged or dysfunctional mitochondria are degraded in lysosomes[37]. The PTEN-induced kinase 1 (PINK1)/Parkin-mediated pathway plays a crucial role in the removal of damaged mitochondria among several mechanisms. PINK1 accumulates on the outer membrane of damaged mitochondria, is autophosphorylated, and phosphorylates ubiquitin, followed by recruitment and activation of the E3 ubiquitin ligase Parkin to induce mitophagy[38–41]. While the conventional CID system allows PINK1 to be recruited to the MOM, followed by mitophagy induction[42], it is challenging to spatiotemporally regulate PINK1 recruitment to the MOM. Since PINK1 accumulation is a regulatory switch in the early events of the PINK1/Parkin-mediated mitophagy pathway, the bidirectional control (recruitment to and diffusion from the MOM) of PINK1 can provide a better understanding of the mitophagy mechanism. Although one optogenetic tool was reported to stimulate mitophagy in a photo-responsive manner[43], this study mainly focused on a pro-autophagy protein unrelated to the PINK1/Parkin pathway, and a method to induce PINK1/Parkin-mediated mitophagy in a photo-responsive manner has yet to be established.

To achieve optical regulation of mitophagy, we fused eDHFR to the cytosolic domain of PINK1 (PINK1Δ1–110, termed cytPINK1)[44] so that cytPINK1 could be recruited to the MOM upon violet light illumination (Fig. 4a). We generated HeLa cells stably expressing a MOM-anchored HaloTag (Halo-OMP25) and a fluorescent marker of the mitochondrial matrix (pSu9-mEGFP) using an IRES sequence. Then, cytPINK1-mOrange2-eDHFR and miRFP670nano-Parkin were transiently co-expressed in HeLa cells, which were treated with 7 μM pcDH. During time-lapse imaging,

stimulation light, typically 405 nm (violet: 130 μW for 100 ms) and 555 nm (green: 1.1 mW for 500 ms), was applied after every image acquisition (Fig. 4b). This intermittent illumination protocol was optimized to suppress the influence of excitation-light-induced photoisomerization because the excitation light for mEGFP (473 nm) may isomerize pcDH. Initially, cytPINK1-mOrange2-eDHFR spread into the cytosol. After the first violet light illumination, cytPINK1-mOrange2-eDHFR was quickly recruited to pSu9-mEGFP-positive mitochondria that expressed Halo-OMP25 on their outer membrane. In contrast, the signals of miRFP670nano-Parkin gradually accumulated in the mitochondria (Fig. 4c,d, Supplementary Video 8), as seen in a previous report on rapalog-induced mitophagy[42]. In the absence of violet light illumination, however, mitochondrial recruitment of either cytPINK1-mOrange2-eDHFR or miRFP670nano-Parkin was not significantly observed (Fig. 4e, Extended Data Fig. 3). In the absence of pcDH, no accumulation of cytPINK1-mOrange2-eDHFR or miRFP670nano-Parkin was observed, regardless of the illumination wavelength (Fig. 4f, Extended Data Fig. 4). Furthermore, we validated the induction of mitophagy by the photochromic CID system using HeLa cells stably expressing MOM-anchored Halo-OMP25 and mEGFP-LC3, a marker of autophagosomes consisting of the microtubule-associated protein light chain 3 (LC3)[45], which resulted in the colocalization of fluorescent puncta of mEGFP-LC3 and miRFP670nano-Parkin accumulated on the MOM after violet light illumination (Extended Data Fig. 5). These results indicated that photochromic CID-based optical recruitment of cytPINK1 on the MOM significantly induced Parkin accumulation on the mitochondria.

The removal of damaged mitochondria by mitophagy requires the accumulation of phosphorylated ubiquitin on the mitochondria[46]. Deubiquitinating enzymes (DUBs) counter the mitophagy pathway by removing ubiquitin chains from the mitochondria (step (i) in Fig. 4a)[47]. Hence, the balance of Parkin and DUBs activities determines whether mitophagic degradation of damaged mitochondria proceeds[48]. Therefore, quantitative regulation of temporal PINK1 recruitment to the mitochondria could provide valuable insights into the mechanism that determines the fate of damaged mitochondria. HeLa cells stably expressing Halo-OMP25 and pSu9-mEGFP were transfected to transiently express cytPINK1-mOrange2-eDHFR and miRFP670nano-Parkin and were treated with 7

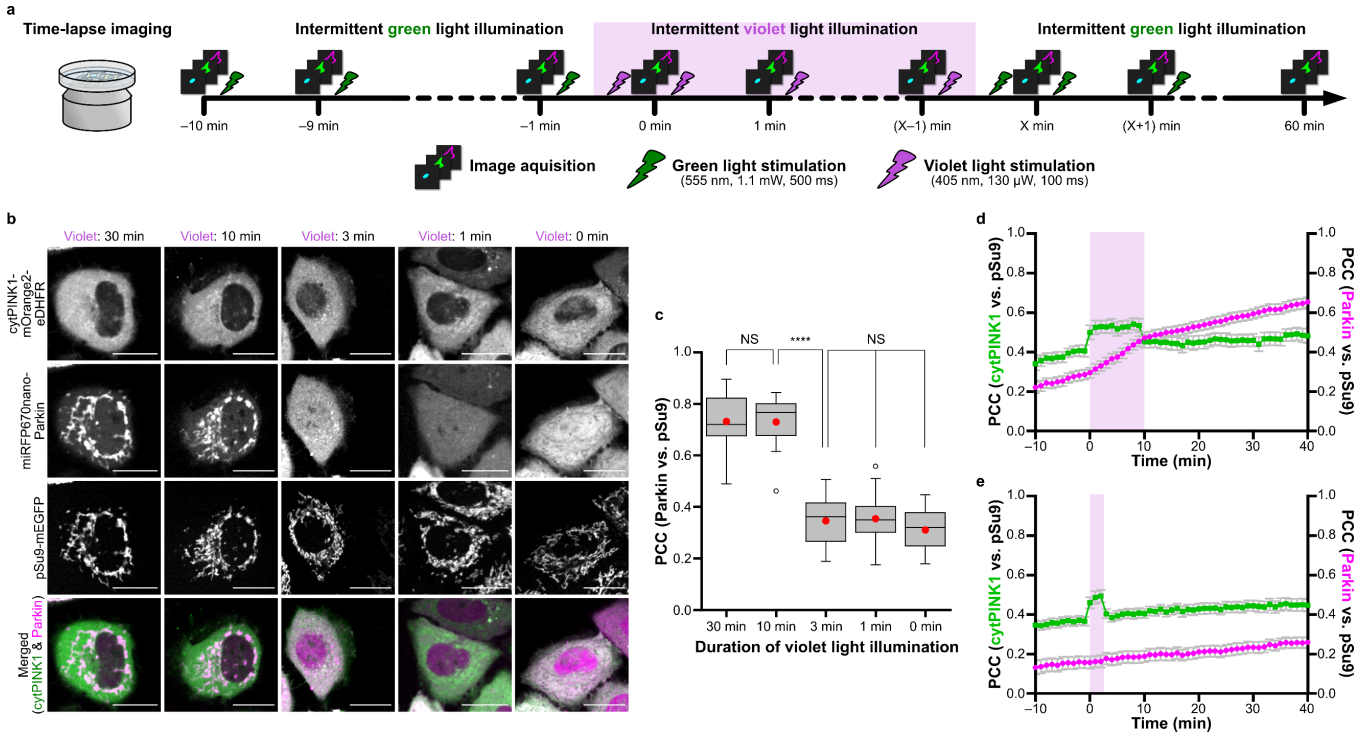

Fig. 5 | Temporal control of cytPINK1 recruitment to the MOM. a, Switching between green- and violet-light illumination to temporally control the anchoring time of cytPINK1 on the MOM. **b**, Confocal fluorescence images of HeLa cells expressing cytPINK1-mOrange2-eDHFR, miRFP670nano-Parkin, pSu9-mEGFP, and Halo-OMP25 at 60 min post-initial violet illumination. **c**, Quantification of Parkin accumulation on the MOM at 60 min post-initial violet illumination. Red dots represent the mean values. Two-tailed Welch's *t*-test. ****$P < 0.0001$ and not significant (NS) for $P > 0.05$. $n = 15$ cells, three independent experiments. **d**,**e**, Time-course changes of PCC between cytPINK1-mOrange2-eDHFR and pSu9-mEGFP (green) or between miRFP670nano-Parkin and pSu9-mEGFP (magenta) with violet light illumination for 10 min (**d**) and 3 min (**e**). Data shown are mean ± s.e.m. Scale bars, 20 μm.

μM pcDH. Then, we temporarily recruited cytPINK1-mOrange2-eDHFR to the MOM by violet light illumination for a certain period and returned cytPINK1 back to the cytosol by subsequent green light illumination (Fig. 5a). Through violet light illumination, a portion of the cytPINK1 protein was transiently localized on the MOM for 30 min, 10 min, 3 min, or 1 min (Extended Data Fig. 6). Although 30-min and 10-min cytPINK1 localization on the MOM induced the accumulation of Parkin on the mitochondria in most cells, shortening the anchoring time of cytPINK1 to 3 min or 1 min significantly depleted Parkin accumulation (Fig. 5b,c). Time-course analysis of the PCC values indicating the mitochondrial localization of the target proteins showed that the accumulation of Parkin on the MOM was accelerated during the transient localization of cytPINK1 on the MOM (Fig. 5d,e). These results demonstrate that the photochromic CID system has achieved fine temporal recruitment of target proteins to specific subcellular regions, and time-dependent data analysis indicated that the PINK1/Parkin-mediated pathway could be regulated by the anchoring time of PINK1 on the MOM.

Discussion

We have developed a photochromic CID system that optically controls the association and dissociation of two genetic tag proteins, eDHFR and HaloTag. Our photochromic CID system showed faster kinetics than the optogenetic dimerization tools (Supplementary Table 1). The observed the half-life $t_{1/2,on}$ (0.78 s) in the bimolecular association process was slightly shorter than or comparable to that of the fastest optogenetic tool, although this process is dependent on the concentrations of both components. Interestingly, the $t_{1/2,off}$ (< 0.3 s) in the unimolecular dissociation process was clearly shorter than that of optogenetic tools (Fig. 2j). Such quick-response photoswitches provide potent tools for temporally refined control of intracellular molecular dynamics, In addition, low-intensity and instantaneous irradiation (60 μW, 100 ms) was sufficient to induce and sustain protein association (Fig. 2b,f,h). Low-intensity and short-duration light illumination can significantly reduce cellular photodamage under sustained protein association. These properties, such as fast-switching kinetics and thermodynamically stable protein association, are attributed to the bistable photoisomers of azobenzene derivatives and can be advantageous over flavin-based optogenetic tools (Supplementary Table 1). Although the chromophores available for optogenetics are limited to natural chromophores such as flavins or bilins, a variety of synthetic photochromic chromophores can be expanded in a semi-infinite chemical space to freely design the spectral and thermodynamic properties.

In addition to temporal regulation, quantitative regulation is crucial for cellular responses in intracellular signaling pathways[11]. A few methods have achieved quantitative protein translocation using caged CID systems[30] or optogenetics[11]. In these cases, the illumination dose was adjusted to control protein translocation levels. However, fine-tuning based on the illumination dose remains challenging, especially for caged CID systems. Because of the irreversible photolysis reaction, once the protein is translocated excessively than expected, it is difficult to reduce the translocation level. The photochromic CID system implemented quantitative and repetitive recruitment of the target protein. Because the photochromic CID system is based on fast and reversible photoisomerization of the ligand, protein recruitment is quantitatively regulated by the fraction of the active *Z* isomer. In this study, we demonstrated quantitative control by the illumination wavelength (Fig. 3b) and intensity ratio of dual-wavelength illumination (Fig. 3e). These single- and dual-wavelength-based regulation methods enabled the control of subcellular protein translocation with prompt response, sufficient duration, quantitativeness, and reversibility.

The photochromic CID system allowed the photoreversible recruitment of PINK1 on the MOM, unlike the traditional FKBP-FRB-based CID technique[40, 42]. This advantage enabled investigation of the relationship between the anchoring time of PINK1 and Parkin accumulation on the MOM. We found that Parkin accumulation was accelerated only when cytPINK1 was anchored to the MOM (Fig. 5d,e). It has been reported that the phosphorylation of Parkin enhances the affinity of Parkin to ubiquitin, and phosphorylated ubiquitin has a higher affinity for phosphorylated Parkin[38,49], leading to Parkin retention on the MOM. Since the phosphorylation levels of MOM proteins are regulated by the balance between phosphorylation by PINK1 and dephosphorylation by DUBs (step (i) in Fig. 4a)[48], the observed acceleration of Parkin recruitment in Fig. 5d,e is likely due to the increased phosphorylation of ubiquitin and Parkin by artificially recruiting cytPINK1 on the MOM. In other words, our photochromic CID technique can manipulate the phosphorylation levels of proteins on the MOM in a photoreversible manner and may eventually be applied to the regulation of other signaling pathways.

We also recognize some drawbacks of this photochromic CID system. The intense excitation light for mEGFP (473 nm) and mOrange2 (555 nm) may cause photoisomerization of pcDH (Fig. 1e, Supplementary Fig. 1). However, this

unfavorable isomerization could be overcome using intermittent illumination (Figs. 4b,5a). This optimized protocol enabled the simultaneous use of various fluorescent proteins in photochromic CID systems. A more critical problem is the K_d difference between 'ON' and 'OFF' states under light illumination. The $K_{d,Dark}/K_{d,394}$ of pcDH to eDHFR was ~3, which was smaller than that of azoMTX (~12-fold)[31]. This is presumably because the two carboxy groups of azoMTX were replaced with -H and -CONHR (R: alkyl group) in pcDH, indicating that either or both negatively charged carboxylates enhanced the binding selectivity for the *Z*-form over the *E*-form. Based on this insight, we are improving the selectivity by derivatization of the photochromic ligand and protein engineering of eDHFR.

In summary, we established a photochromic CID system, a novel methodology for the fine control of intracellular protein localization, and demonstrated the photoreversible manipulation of intracellular molecular networks associated with mitophagy. The photochromic CID strategy can not only be used as an alternative to optogenetic tools or caged CID systems, but also has a high potential for unique applications because of the exceedingly high temporal resolution and the small size of the protein tags (eDHFR: 18 kDa and HaloTag: 33 kDa). In the future, the photochromic CID strategy will open a new gateway to controlling the intracellular dynamics of endogenous proteins by light. In principle, endogenous proteins can be photoreversibly recruited to intracellular compartments, where eDHFR is expressed using a bifunctional dimerizer consisting of a specific ligand for an endogenous target protein and a photochromic eDHFR ligand. It is also promising to utilize a covalent labeling strategy for endogenous proteins[50]. We envision that a photochromic ligand-based strategy will expand the toolbox for the spatiotemporal control of intracellular protein dynamics and contribute to broad fields of cell biology.

REFERENCES

1. Lavoie, H. & Therrien, M. Regulation of RAF protein kinases in ERK signalling. *Nat. Rev. Mol. Cell Biol.* **16**, 281–298 (2015).
2. Stanton, B.Z., Chory, E.J. & Crabtree, G.R. Chemically induced proximity in biology and medicine. *Science* **359**, eaao5902 (2018).
3. Passmore, J.B., Nijenhuis, W. & Kapitein, L.C. From observing to controlling: Inducible control of organelle dynamics and interactions. *Curr. Opin. Cell Biol.* **71**, 69–76 (2021).
4. Tei, R. & Baskin, J.M. Induced proximity tools for precise manipulation of lipid signaling. *Curr. Opin. Chem. Biol.* **65**, 93–100 (2021).
5. Klewer, L. & Wu, Y.-W. Light-Induced Dimerization Approaches to Control Cellular Processes. *Chem. Eur. J.* **25**, 12452–12463 (2019).
6. Levskaya, A., Weiner, O.D., Lim, W.A. & Voigt, C.A. Spatiotemporal control of cell signalling using a light-switchable protein interaction. *Nature* **461**, 997–1001 (2009).
7. Kennedy, M.J. et al. Rapid blue-light–mediated induction of protein interactions in living cells. *Nat. Methods* **7**, 973–975 (2010).
8. Guntas, G. et al. Engineering an improved light-induced dimer (iLID) for controlling the localization and activity of signaling proteins. *Proc. Natl. Acad. Sci. USA* **112**, 112–117 (2015).
9. Kawano, F., Suzuki, H., Furuya, A. & Sato, M. Engineered pairs of distinct photoswitches for optogenetic control of cellular proteins. *Nat. Commun.* **6**, 6256 (2015).
10. Farahani, P.E., Reed, E.H., Underhill, E.J., Aoki, K. & Toettcher, J.E. Signaling, Deconstructed: Using Optogenetics to Dissect and Direct Information Flow in Biological Systems. *Annu. Rev. Biomed. Eng.* **23**, 61–87 (2021).
11. Toettcher, Jared E., Weiner, Orion D. & Lim, Wendell A. Using Optogenetics to Interrogate the Dynamic Control of Signal Transmission by the Ras/Erk Module. *Cell* **155**, 1422–1434 (2013).
12. Bugaj, L.J. et al. Cancer mutations and targeted drugs can disrupt dynamic signal encoding by the Ras-Erk pathway. *Science* **361**, eaao3048 (2018).
13. Ma, G. et al. Optogenetic engineering to probe the molecular choreography of STIM1-mediated cell signaling. *Nat. Commun.* **11**, 1039 (2020).
14. Taslimi, A. et al. Optimized second-generation CRY2–CIB dimerizers and photoactivatable Cre recombinase. *Nat. Chem. Biol.* **12**, 425–430 (2016).
15. Toettcher, J.E., Gong, D., Lim, W.A. & Weiner, O.D. Light-based feedback for controlling intracellular signaling dynamics. *Nat. Methods* **8**, 837–839 (2011).
16. Kaberniuk, A.A., Shemetov, A.A. & Verkhusha, V.V. A bacterial phytochrome-based optogenetic system controllable with near-infrared light. *Nat. Methods* **13**, 591–597 (2016).
17. Belshaw, P.J., Ho, S.N., Crabtree, G.R. & Schreiber, S.L. Controlling protein association and subcellular localization with a synthetic ligand that induces heterodimerization of proteins. *Proc. Natl. Acad. Sci. USA* **93**, 4604–4607 (1996).
18. Rutkowska, A. & Schultz, C. Protein Tango: The Toolbox to Capture Interacting Partners. *Angew. Chem. Int. Ed.* **51**, 8166–8176 (2012).
19. Pecot, M.Y. & Malhotra, V. Golgi Membranes Remain Segregated from the Endoplasmic Reticulum during Mitosis in Mammalian Cells. *Cell* **116**, 99–107 (2004).
20. Karginov, A.V. et al. Light Regulation of Protein Dimerization and Kinase Activity in Living Cells Using Photocaged Rapamycin and Engineered FKBP. *J. Am. Chem. Soc.* **133**, 420–423 (2011).
21. Wright, C.W., Guo, Z.-F. & Liang, F.-S. Light Control of Cellular Processes by Using Photocaged Abscisic Acid. *ChemBioChem* **16**, 254–261 (2015).
22. Schelkle, K.M. et al. Light-Induced Protein Dimerization by One- and Two-Photon Activation of Gibberellic Acid Derivatives in Living Cells. *Angew. Chem. Int. Ed.* **54**, 2825–2829 (2015).
23. Ballister, E.R., Aonbangkhen, C., Mayo, A.M., Lampson, M.A. & Chenoweth, D.M. Localized light-induced protein dimerization in living cells using a photocaged dimerizer. *Nat. Commun.* **5**, 5475 (2014).
24. Zimmermann, M. et al. Cell-Permeant and Photocleavable Chemical Inducer of Dimerization. *Angew. Chem. Int. Ed.* **53**, 4717–4720 (2014).
25. Brown, K.A. et al. Light-cleavable rapamycin dimer as an optical trigger for protein dimerization. *Chem. Commun.* **51**, 5702–5705 (2015).
26. Kowada, T. et al. Optical Manipulation of Subcellular Protein Translocation Using a Photoactivatable Covalent Labeling System. *Angew. Chem. Int. Ed.* **60**, 11378–11383 (2021).

27. Zhang, H. et al. Optogenetic control of kinetochore function. *Nat. Chem. Biol.* **13**, 1096–1101 (2017).
28. Akera, T. et al. Spindle asymmetry drives non-Mendelian chromosome segregation. *Science* **358**, 668–672 (2017).
29. Aonbangkhen, C., Zhang, H., Wu, D.Z., Lampson, M.A. & Chenoweth, D.M. Reversible Control of Protein Localization in Living Cells Using a Photocaged-Photocleavable Chemical Dimerizer. *J. Am. Chem. Soc.* **140**, 11926–11930 (2018).
30. Chen, X. & Wu, Y.-W. Tunable and Photoswitchable Chemically Induced Dimerization for Chemo-optogenetic Control of Protein and Organelle Positioning. *Angew. Chem. Int. Ed.* **57**, 6796–6799 (2018).
31. Mashita, T., Kowada, T., Takahashi, H., Matsui, T. & Mizukami, S. Light-Wavelength-Based Quantitative Control of Dihydrofolate Reductase Activity by Using a Photochromic Isostere of an Inhibitor. *ChemBioChem* **20**, 1382–1386 (2019).
32. Matera, C. et al. Photoswitchable Antimetabolite for Targeted Photoactivated Chemotherapy. *J. Am. Chem. Soc.* **140**, 15764–15773 (2018).
33. Los, G.V. et al. HaloTag: A Novel Protein Labeling Technology for Cell Imaging and Protein Analysis. *ACS Chem. Biol.* **3**, 373–382 (2008).
34. Baccanari, D.P., Daluge, S. & King, R.W. Inhibition of dihydrofolate reductase: effect of NADPH on the selectivity and affinity of diaminobenzylpyrimidines. *Biochemistry* **21**, 5068–5075 (1982).
35. Benedetti, L. et al. Light-activated protein interaction with high spatial subcellular confinement. *Proc. Natl. Acad. Sci. USA* **115**, E2238–E2245 (2018).
36. Benedetti, L. et al. Optimized Vivid-derived Magnets photodimerizers for subcellular optogenetics in mammalian cells. *eLife* **9**, e63230 (2020).
37. Palikaras, K., Lionaki, E. & Tavernarakis, N. Mechanisms of mitophagy in cellular homeostasis, physiology and pathology. *Nat. Cell Biol.* **20**, 1013–1022 (2018).
38. Ordureau, A. et al. Quantitative Proteomics Reveal a Feedforward Mechanism for Mitochondrial PARKIN Translocation and Ubiquitin Chain Synthesis. *Mol. Cell* **56**, 360–375 (2014).
39. Kane, L.A. et al. PINK1 phosphorylates ubiquitin to activate Parkin E3 ubiquitin ligase activity. *J. Cell Biol.* **205**, 143–153 (2014).
40. Okatsu, K. et al. PINK1 autophosphorylation upon membrane potential dissipation is essential for Parkin recruitment to damaged mitochondria. *Nat. Commun.* **3**, 1016 (2012).
41. Gan, Z.Y. et al. Activation mechanism of PINK1. *Nature* **602**, 328–335 (2022).
42. Lazarou, M., Jin, Seok M., Kane, Lesley A. & Youle, Richard J. Role of PINK1 Binding to the TOM Complex and Alternate Intracellular Membranes in Recruitment and Activation of the E3 Ligase Parkin. *Dev. Cell* **22**, 320–333 (2012).
43. D'Acunzo, P. et al. Reversible induction of mitophagy by an optogenetic bimodular system. *Nat. Commun.* **10**, 1533 (2019).
44. Narendra, D.P. et al. PINK1 Is Selectively Stabilized on Impaired Mitochondria to Activate Parkin. *PLoS Biol.* **8**, e1000298 (2010).
45. Kabeya, Y. et al. LC3, a mammalian homologue of yeast Apg8p, is localized in autophagosome membranes after processing. *EMBO J.* **19**, 5720–5728 (2000).
46. Lazarou, M. et al. The ubiquitin kinase PINK1 recruits autophagy receptors to induce mitophagy. *Nature* **524**, 309–314 (2015).
47. Bingol, B. et al. The mitochondrial deubiquitinase USP30 opposes parkin-mediated mitophagy. *Nature* **510**, 370–375 (2014).
48. Harper, J.W., Ordureau, A. & Heo, J.-M. Building and decoding ubiquitin chains for mitophagy. *Nat. Rev. Mol. Cell Biol.* **19**, 93–108 (2018).
49. Ordureau, A. et al. Defining roles of PARKIN and ubiquitin phosphorylation by PINK1 in mitochondrial quality control using a ubiquitin replacement strategy. *Proc. Natl. Acad. Sci. USA* **112**, 6637–6642 (2015).
50. Tamura, T. et al. Rapid labelling and covalent inhibition of intracellular native proteins using ligand-directed N-acyl-N-alkyl sulfonamide. *Nat. Commun.* **9**, 1870 (2018).

Methods

pcDH, TMP-Fl, and TMP-HTL synthesis. The synthetic procedures are provided in the Supplementary Note.

***In vitro* pcDH characterization.** UV/vis absorption spectra and time-dependent absorption changes were recorded on a UV-2450 spectrophotometer (Shimadzu, Tokyo, Japan) with the slit width set to 1 nm. pcDH (20 μM) was incubated at 37 °C for 1 h in 100 mM HEPES-NaOH buffer (pH 7.4) containing 100 mM NaCl and 1% DMSO before the measurement. For the photoisomerization analysis of pcDH, light irradiation was performed using a xenon light source (MAX-303, Asahi Spectra Co., Ltd., Tokyo, Japan) equipped with bandpass filters (330/10, 365/10, 394/10, 440/10, 450/10, 488/10, 515/10, and 560/10) at room temperature (5.0 mW cm^{-2}).

High-performance liquid chromatography (HPLC) analyses were performed with an Inertsil ODS-3 column (4.6 mm × 250 mm, GL-Science, Tokyo, Japan) using an HPLC system comprising a pump (PU-2080, JASCO, Tokyo, Japan) and a detector (MD-2010, JASCO), and the absorbance was monitored at 264 and 414 nm, which were isosbestic points of pcDH in the eluent. Eluent A was composed of 0.1% formic acid in water. Eluent B was composed of 0.1% formic acid in acetonitrile. pcDH (100 μM) was incubated at 37 °C for 1 h in 100 mM HEPES-NaOH buffer (pH 7.4) containing 3% DMSO before the measurement. Light irradiation was performed using a xenon light source at room temperature (5.0 mW cm^{-2}).

The binding affinities of TMP-Fl and pcDH were determined using fluorescence polarization recorded on a multimode plate reader (Nivo, PerkinElmer, Waltham, MA, USA). The excitation and emission wavelengths were set to 480/30 and 530/30 nm, respectively. To determine the dissociation constant of the eDHFR–TMP-Fl complex ($K_{d,L}$), a mixture of eDHFR, TMP-Fl (1.5 nM), and NADPH (5.0 μM) was incubated at 37 °C for 15 min in 100 mM HEPES-NaOH buffer (pH 7.4) containing 100 mM NaCl before the measurements. The $K_{d,L}$ value was determined from the plot obtained using Equation (1).

$$P = P_{min} + (P_{max} - P_{min}) \times (([L]_T + [P]_T + K_{d,L}) - \mathrm{sqrt}\{([L]_T + [P]_T + K_{d,L})^2 - 4[P]_T[L]_T\}) / 2[L]_T, \quad (1)$$

where P is the fluorescence polarization at each eDHFR concentration, P_{min} is the minimum fluorescence polarization, P_{max} is the maximum fluorescence polarization, $[L]_T$ is the total concentration of TMP-Fl, and $[P]_T$ is the total concentration of eDHFR.

To determine the dissociation constant of the eDHFR–pcDH complex, a mixture of pcDH, TMP-Fl (1.5 nM), eDHFR (2.0 nM), and NADPH (5.0 μM) was incubated at 37 °C for 45 min in 100 mM HEPES-NaOH buffer (pH 7.4) containing 100 mM NaCl before the measurements. pcDH was irradiated with 394/10 nm light (5.0 mW cm^{-2}) at room temperature to obtain pcDH under 394 nm irradiation before mixing with other components. IC_{50} values were determined from the plot obtained using Equation (2).

$$P = P_{min} + (P_{max} - P_{min}) / (1 + ([\mathrm{pcDH}] / IC_{50})) \quad (2)$$

where P is fluorescence polarization at each pcDH concentration, P_{max} is fluorescence polarization without pcDH, and P_{min} is minimum fluorescence polarization.

The dissociation constant (K_d) was calculated from the determined IC_{50} value using the Nikolovska-Coleska equation[51] (3).

$$K_d = [I]_{50} / \{([L]_{50} / K_{d,L}) + ([P]_0 / K_{d,L}) + 1\} \quad (3)$$

, where $[I]_{50}$ is the concentration of pcDH at 50% inhibition, $[L]_{50}$ is the concentration of free TMP-Fl at 50% inhibition, $[P]_0$ is the concentration of free eDHFR at 0% inhibition, and $K_{d,L}$ is the dissociation constant of the eDHFR–TMP-Fl complex ($K_{d,L}$ = 0.25 nM, Supplementary Fig. 3).

DNA plasmid construction. Synthetic genes encoding mOrange2, miRFP670nano, and Parkin were purchased from Eurofins Genomics (Tokyo, Japan). The gene encoding cytPINK1 was obtained from pcDNA-DEST47 PINK1 C-GFP (#13316; Addgene, Cambridge, MA, USA) using a standard PCR method (Takara Bio, Shiga, Japan).

The plasmids for recombinant eDHFR and HaloTag expression were prepared as previously described[31, 52].

For eDHFR-miRFP670nano, the gene encoding the fusion protein of eDHFR and miRFP670nano was inserted into the NheI/EcoRI site of a pcDNA3.1(+) vector (Invitrogen, Carlsbad, CA, USA). A single HindIII site and three amino acids (AAA) were inserted between the eDHFR and miRFP670nano sequences. For nuclear export, the human immunodeficiency virus-1 Rev protein nuclear export sequence (NES: LQLPPLERLTL)[53] was incorporated at the C-terminus of miRFP670nano, and a single BamHI site and eight amino acids (QLGGSGGS) were inserted between miRFP670nano and NES sequences.

For nuclear-targeting Halo-mOrange2, three copies of the simian virus 40 (SV40) large T-antigen nuclear localization sequence (NLS: PKKKRKVDPKKKRKVDPKKKRKV)[54] were incorporated at the C-terminus of the fusion protein of HaloTag and mOrange2. A single HindIII site was inserted between the Halo and mOrange2 sequences, and a single BamHI site and six amino acids (GGSGGS) were inserted between the mOrange2 and NLS sequences. The gene encoding the Halo-mOrange2-NLS was inserted into the NheI/EcoRI site of the pcDNA3.1(+) vector. For anchoring Halo-mOrange2 to the cytosolic interface of the plasma membrane, the CAAX sequence of Kras (KKKKKKSKTKCVIM)[55] was incorporated at the C-terminus of the fusion protein of HaloTag and mOrange2. A single BamHI site and amino acid (G) were inserted between the mOrange2 and CAAX sequences. For ER targeting, the ER-targeting domain of cytochrome *b5* (Cb5; amino acids 100–134)[56] was incorporated at the C-terminus of the fusion protein of HaloTag and mOrange2. A single BamHI site and four amino acids (GGGS) were inserted between mOrange2 and Cb5 sequences. For MOM targeting, the mitochondria-targeting domain of Tom20 (amino acids 1–33)[57] was incorporated into the N-terminus of the fusion protein of mOrange2 and HaloTag. There was only a single BamHI site between the mOrange2 and Halo sequences, and only a single HindIII site between the Tom20 and mOrange2 sequences. The gene encoding Tom20-mOrange2-Halo was inserted into the NheI/EcoRI site of pcDNA3.1(+) vector.

For cytPINK1-mOrange2-eDHFR, the gene encoding cytPINK1-mOrange2-eDHFR was inserted into the NheI/EcoRI site of pcDNA3.1(+) vector. A 2×GGGS flexible linker was inserted at the AflII/BamHI site between cytPINK1 and mOrange2. The V5-tag sequence was incorporated into the C-terminus of the fusion protein. Two amino acids (GS) and a single HindIII site were inserted between the mOrange2 and eDHFR sequences, whereas a single SacII site and

four amino acids (GGGS) were inserted between the eDHFR and V5-tag sequences.

For Parkin-miRFP670nano, the gene encoding Parkin-miRFP670nano was inserted into the NheI/EcoRI site of pcDNA3.1(+) vector. The HA-tag sequence was incorporated into the N terminus of the fusion protein. There was only a single HindIII site between the HA-tag and miRFP670nano sequences, and only a single BamHI site between the miRFP670nano and Parkin sequences.

Retroviral plasmids for co-expression of Halo-OMP25 with pSu9-mEGFP or mEGFP-rLC3B were generated as follows: the genes encoding HaloTag7 (N2701; Promega, Madison, WI, USA) and the transmembrane domain of rat OMP25 (residues 109–145) were inserted into the HindIII/XhoI site of the retroviral plasmid pMRX-IP[58,59] using the SLiCE method[60], resulting in the generation of pMRX-Halo-OMP25-IRES-Puro. The genes encoding monomeric enhanced GFP (mEGFP) and the presequence of *Neurospora crassa* Fo-ATPase subunit 9 (pSu9) (residues 1–69) or rat LC3B were inserted into the SalI site of pMRX-Halo-OMP25-IRES-Puro using the SLiCE method[60] to replace the puromycin-resistant marker, resulting in the generation of pMRX-Halo-OMP25-IRES-pSu9-mEGFP and pMRX-Halo-OMP25-IRES-mEGFP-rLC3B.

All plasmids were verified using Sanger sequencing.

Recombinant protein expression and purification. Recombinant eDHFR and HaloTag were expressed and purified aspreviously described[31,52].

Stable cell line generation. To stably express Halo-OMP25 with pSu9-mEGFP or mEGFP-rLC3B in HeLa cells, retroviral solutions were prepared as follows. HEK293T cells were transfected with pMRX-Halo-OMP25-IRES-pSu9-mEGFP or pMRX-Halo-OMP25-IRES-mEGFP-rLC3B together with pCG-gag-pol and pCG-VSV-G using Lipofectamine 2000 (11668019; Thermo Fisher Scientific, Waltham, MA, USA). After the cells were cultured for 2 d in Dulbecco's modified Eagle's medium (DMEM) (Nacalai Tesque, Kyoto, Japan), the retrovirus-containing medium was harvested, filtered through a 0.45-μm filter unit (Ultrafree-MC; Millipore, Bedford, MA, USA), and added to HeLa cells with 8 μg/mL polybrene (H9268; Sigma-Aldrich, St. Louis, MO, USA). After the cells were cultured for 1 d, selection was performed using 1 μg/mL puromycin (P8833; Sigma-Aldrich).

Cell culture and transfection. HeLa cells (RCB0007) were cultured in minimum essential medium (MEM, Nacalai Tesque) supplemented with 10% fetal bovine serum (FBS, Nichirei Biosciences, Tokyo, Japan), 100 U/mL penicillin, and 100 μg/mL streptomycin (Nacalai Tesque) at 37 °C in a humidified incubator with 5% CO_2. Three days before imaging, the cells were seeded on 35-mm glass-bottomed dishes (AGC Techno Glass, Shizuoka, Japan) in antibiotic-free MEM supplemented with 10% FBS. After 24 h, transfection was performed using FuGENE HD (Promega), according to the manufacturer's protocols, with plasmid DNA and FuGENE HD at a 1:7 ratio in Opti-MEM (Gibco, Grand Island, NY, USA).

Live-cell imaging. All images were acquired using an inverted IX83 microscope (Olympus, Tokyo, Japan) equipped with a ×60/1.49 numerical aperture (NA) oil objective (APON 60XOTIRF, Olympus), a multi-wavelength laser diode light source (LDI-7, 89 North, Williston, VT, USA), a spinning-disk unit (CSU-W1, Yokogawa Electric, Tokyo, Japan), and an ORCA-Fusion BT CMOS camera (Hamamatsu Photonics, Hamamatsu, Japan). The microscope was driven by MetaMorph 7.10 software (Molecular Devices, San Jose, CA, USA). mEGFP images were acquired using a 470-nm laser, a 405/488/561/640 dichroic mirror, and a 525/50 emission filter. mOrange2 images were acquired using a 555-nm laser, 405/488/561/640 dichroic mirror, and 600/50 emission filter. miRFP670nano images were acquired using a 640-nm laser, a 405/488/561/640 dichroic mirror, and a 700/75 emission filter. The cells were maintained in a controlled-environment chamber (Incubator System T, LCI, Namyangju-si, Korea) at 37 °C during imaging.

Photoreversible protein translocation assay. HeLa cells were plated at 5.0×10^4 cells per dish and transfected with four pairs of plasmids (cytosolic interface of plasma membrane: pcDNA3.1(+)-eDHFR-miRFP670nano-NES and pcDNA3.1(+)-Halo-mOrange2-CAAX; nucleus: pcDNA3.1(+)-eDHFR-miRFP670nano and pcDNA3.1(+)-Halo-mOrange2-NLS; MOM: pcDNA3.1(+)-eDHFR-miRFP670nano-NES and pcDNA3.1(+)-Tom20-mOrange2-Halo; cytosolic interface of ER membrane: pcDNA3.1(+)-eDHFR-miRFP670nano-NES and pcDNA3.1(+)-Halo-mOrange2-Cb5). The ratios of the plasmids used were 1:2 (eDHFR-miRFP670nano-NES/Halo-mCherry-CAAX, eDHFR-miRFP670nano/Halo-mCherry-NLS) and 2:3 (eDHFR-miRFP670nano-NES/Tom20-mOrange2-Halo, eDHFR-miRFP670nano-NES/Halo-mOrange2-Cb5). After 36 h of transfection, the cells were washed twice with Hanks' Balanced Salt Solution (HBSS (+)) and treated with 5 μM pcDH (plasma membrane and ER) or 3 μM pcDH (nucleus and mitochondria) in DMEM for 1 h. Culture medium was replaced with HBSS (+). Fluorescence images were acquired every 30 s for 40 min (plasma membrane, MOM, and ER) and every 1 min for 70 min (nucleus). Violet and green light illumination were performed using a multi-wavelength laser diode at 405 nm (60 μW for 100 ms) and 555 nm (1.1 mW for 500 ms), respectively. For the TMP competition assay, 200 μL HBSS (+) containing 500 μM TMP (final concentration of 50 μM) was added 20 min after the initial image acquisition. Fluorescence images were acquired every 30 s for 30 min.

Analysis of mitochondrial recruitment rate. HeLa cells were plated at 5.0×10^4 cells per dish and transfected with plasmids encoding eDHFR-miRFP670nano-NES and Tom20-mOrange2-Halo at 2:3 ratio. After 36 h of transfection, the cells were washed twice with HBSS (+) and treated with 3 μM pcDH in DMEM for 1 h. The culture medium was replaced with HBSS (+). Fluorescence images were acquired every 300 ms for 30 s. Violet and green light illumination were performed using a multi-wavelength laser diode at 405 nm (60 μW for 100 ms) and 555 nm (1.4 mW for 100 ms), respectively.

Quantitative protein translocation assay. HeLa cells were

plated at 5.0×10^4 cells per dish and transfected with plasmids encoding eDHFR-miRFP670nano-NES and Halo-mOrange2-CAAX at 1:2 ratio. After 36 h of transfection, the cells were washed twice with HBSS (+) and treated with 5 μM pcDH in DMEM for 1 h. The culture medium was replaced with HBSS (+). Fluorescence images were acquired every 30 s for 45 min for the quantitative recruitment assay using different wavelengths of light. Violet, blue, and green light illumination were performed with a multi-wavelength laser diode at 405 nm (60 μW for 100 ms), 445 nm (130 μW for 300 ms), and 555 nm (1.1 mW for 500 ms), respectively. For the quantitative recruitment assay using a combination of violet and green light, fluorescence images were acquired every 30 s for 51 min. Violet (382.5–394.5 nm) and green (543–557.5 nm) light illumination were performed using a solid-state LED light source (SPECTRA X Light Engine, Lumencor, Beaverton, OR, USA). To recruit cytosolic eDHFR to the plasma membrane, violet (42 μW) and green lights with different ratios (1:0, 1:19, 1:31, and 1:92) were simultaneously illuminated for 500 ms to the cells. For cancellation of protein dimerization, only green light (1.1 mW for 500 ms) was illuminated.

For the quantitative recruitment assay using a conventional chemical dimerizer, 0.5 or 5.0 μM TMP-HTL was used instead of the pcDH. After treatment with TMP-HTL, the culture medium was replaced with HBSS (+), and fluorescence images were acquired.

Photoregulation of mitophagy using the photochromic CID system. HeLa cells stably expressing Halo-OMP25 and pSu9-mEGFP or those stably expressing Halo-OMP25 and mEGFP-rLC3B were plated at 4.0×10^4 cells per dish and transfected with plasmids encoding cytPINK1-mOrange2-eDHFR and miRFP670nano-Parkin at 3:5 ratio. After 36 h of transfection, the cells were washed twice with HBSS (+) and treated with 7 μM pcDH in DMEM for 30 min. Before imaging, the culture medium was replaced with fresh DMEM supplemented with 10% FBS. Fluorescence images were acquired every 1 min for 70 min. Violet and green light illumination were performed using a multi-wavelength laser diode at 405 nm (130 μW for 100 ms) and 555 nm (1.1 mW for 500 ms), respectively.

Cytosolic protein recruitment analysis. All image analysis was performed with the open-source software Fiji[61] (Fiji is ImageJ). The regions of interest (ROIs) for the nucleus and mitochondria were defined by thresholding the mOrange2 signals to determine fluorescence intensity in the organelles. PCC was determined for individual cells using the EzColocalization[62] plugin in Fiji.

Analysis of recruitment rate to mitochondria. Fluorescence intensities from ROIs defined by thresholding Tom20-Halo-mOrange2 signals were fitted to the following mono-exponential equation (4):

$$F = \mathrm{A}e^{-kt} + \mathrm{B} \quad (4)$$

where F is the fluorescence intensity in the ROI at time t, A and B are parameters, and k is the rate constant. The half-life, $t_{1/2}$, was determined using Equation (5).

$$t_{1/2} = \ln 2 / k \quad (5)$$

Statistical analysis. Unless otherwise stated, most statistical analyses were performed with two-tailed Welch's *t*-tests using Microsoft Excel. A paired two-tailed Student's *t*-test was used in Fig. 3c. KaleidaGraph (Synergy Software) was used for data plotting. For box plots, the red dot indicates the mean values, the middle line indicates the median, the box limits indicate 25th and 75th percentiles, the whiskers extend to the maximum and minimum, and the data falling more than 1.5 times the interquartile range from the box are considered as outliers and shown with a white circle.

Material availability. Plasmid DNAs generated in this study are available from the corresponding author upon reasonable request.

Data availability

All data are available from the corresponding author upon reasonable request.

Acknowledgements

This work was supported by JSPS and MEXT KAKENHI (Nos. JP19H05284, JP20K05702, JP21H05252, and JP21H05256), Takeda Science Foundation, Nakatani Foundation, Inamori Foundation, AMED-CREST (21gm1410006h0001), and the "Dynamic Alliance for Open Innovation Bridging Human, Environment and Materials" Research Program in the "Network Joint Research Center for Materials and Devices". We thank the Tagen Central Analytical Facility for providing the NMR and MS instruments. We are grateful to Shoji Yamaoka for the pMRXIP plasmid, and Teruhito Yasui for the pCG-gag-pol and pCG-VSV-G plasmids.

References

51. Nikolovska-Coleska, Z. et al. Development and optimization of a binding assay for the XIAP BIR3 domain using fluorescence polarization. *Anal. Biochem.* **332**, 261–273 (2004).
52. Kowada, T. et al. Quantitative Imaging of Labile Zn^{2+} in the Golgi Apparatus Using a Localizable Small-Molecule Fluorescent Probe. *Cell Chem. Biol.* **27**, 1521–1531.e8 (2020).
53. Wen, W., Meinkoth, J.L., Tsien, R.Y. & Taylor, S.S. Identification of a Signal for Rapid Export of Proteins from the Nucleus. *Cell* **82**, 463–473 (1995).
54. Kalderon, D., Roberts, B.L., Richardson, W.D. & Smith, A.E. A short amino acid sequence able to specify nuclear location. *Cell* **39**, 499–509 (1984).
55. Choy, E. et al. Endomembrane Trafficking of Ras: The CAAX Motif Targets Proteins to the ER and Golgi. *Cell* **98**, 69–80 (1999).
56. Komatsu, T. et al. Organelle-specific, rapid induction of molecular activities and membrane tethering. *Nat. Methods* **7**, 206–208 (2010).
57. Kanaji, S., Iwahashi, J., Kida, Y., Sakaguchi, M. & Mihara, K. Characterization of the Signal That Directs Tom20 to the Mitochondrial Outer Membrane. *J. Cell Biol.* **151**, 277–288 (2000).
58. Saitoh, T. et al. TWEAK Induces NF-κB2 p100 Processing and Long Lasting NF-κB Activation. *J. Biol. Chem.* **278**, 36005–36012 (2003).
59. Kitamura, T. et al. Retrovirus-mediated gene transfer and expression cloning: powerful tools in functional genomics. *Exp. Hematol.* **31**, 1007–1014 (2003).
60. Motohashi, K. in In Vitro Mutagenesis: Methods and Protocols. (ed. A. Reeves) 349–357 (Springer New York, New York, NY; 2017).
61. Schindelin, J. et al. Fiji: an open-source platform for biological-image analysis. *Nat. Methods* **9**, 676–682 (2012).

62. Stauffer, W., Sheng, H. & Lim, H.N. EzColocalization: An ImageJ plugin for visualizing and measuring colocalization in cells and organisms. *Sci. Rep.* **8**, 15764 (2018).

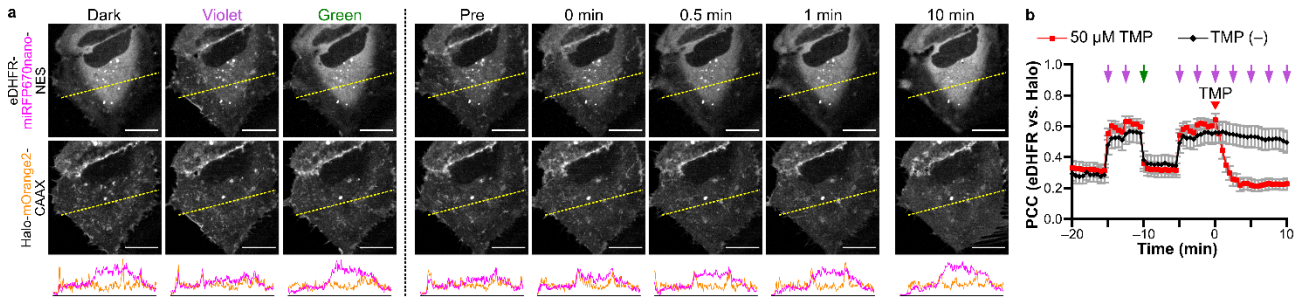

Extended Data Fig. 1 | Suppression of recruitment to the plasma membrane upon addition of TMP. a, Photochromism-induced recruitment of cytosolic proteins to the plasma membrane followed by diffusion by the addition of TMP. Confocal fluorescence images of HeLa cells expressing Halo-mOrange2-CAAX and eDHFR-miRFP670nano-NES before and after illumination at 405 nm (violet) and 555 nm (green). **b**, Time-course changes in the PCC. Arrows indicate light irradiation at 405 nm (violet) and 555 nm (green). The addition of TMP (final concentration: 50 μM, red triangle) at 0 min induced eDHFR diffusion from the plasma membrane to the cytosol, the rate of which was slower than the rate of diffusion induced by the green light (green arrow at −10 min). Data shown are the mean ± s.e.m., *n* = 13 cells (50 μM TMP) or 14 cells (TMP (−)), three independent experiments. Scale bar, 20 μm.

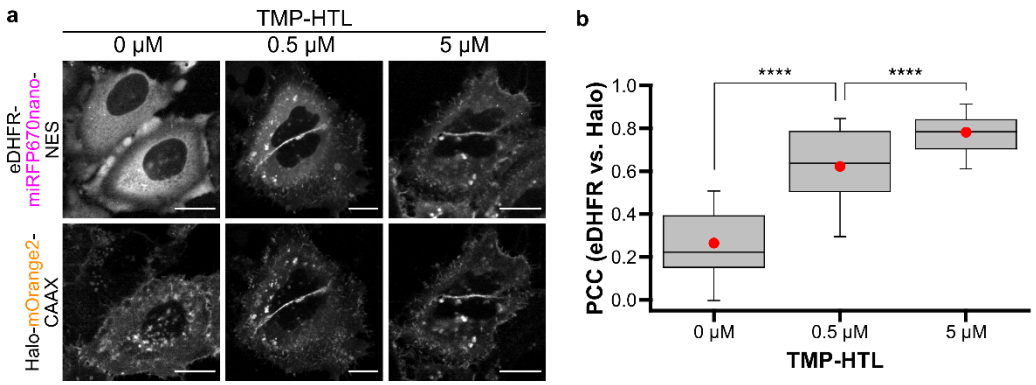

Extended Data Fig. 2 | Quantitative recruitment of cytosolic proteins induced by different concentrations of TMP-HTL. **a**, Recruitment of cytosolic proteins to the plasma membrane upon addition of the conventional chemical dimerizer TMP-HTL. Confocal fluorescence images of HeLa cells expressing Halo-mOrange2-CAAX and eDHFR-miRFP670nano-NES treated with 0, 0.5, or 5 μM TMP-HTL. **b**, Quantification of eDHFR recruitment using TMP-HTL. The red dots represent mean values. Two-tailed Welch's *t*-tests were performed. ****$P < 0.0001$; $n = 26$ cells (0 μM), 25 cells (0.5 μM), or 34 cells (5 μM), respectively; three independent experiments. Scale bars, 20 μm.

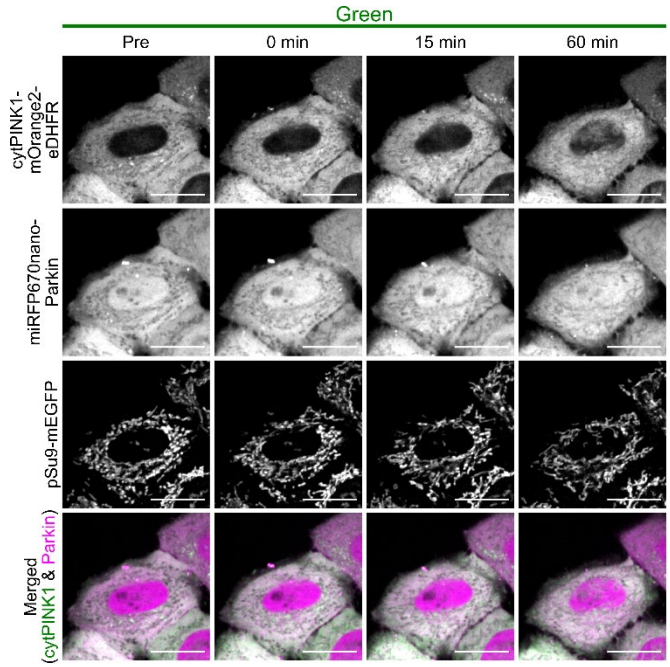

Extended Data Fig. 3 | Optical regulation of mitophagy by the photochromic CID system. Confocal fluorescence images of HeLa cells expressing cytPINK1-mOrange2-eDHFR, miRFP670nano-Parkin, pSu9-mEGFP, and Halo-OMP25. Green light (555 nm) was illuminated after every image acquisition to suppress the recruitment of cytPINK1-mOrange2-eDHFR by the excitation light. Scale bar, 20 μm. Three independent experiments were performed.

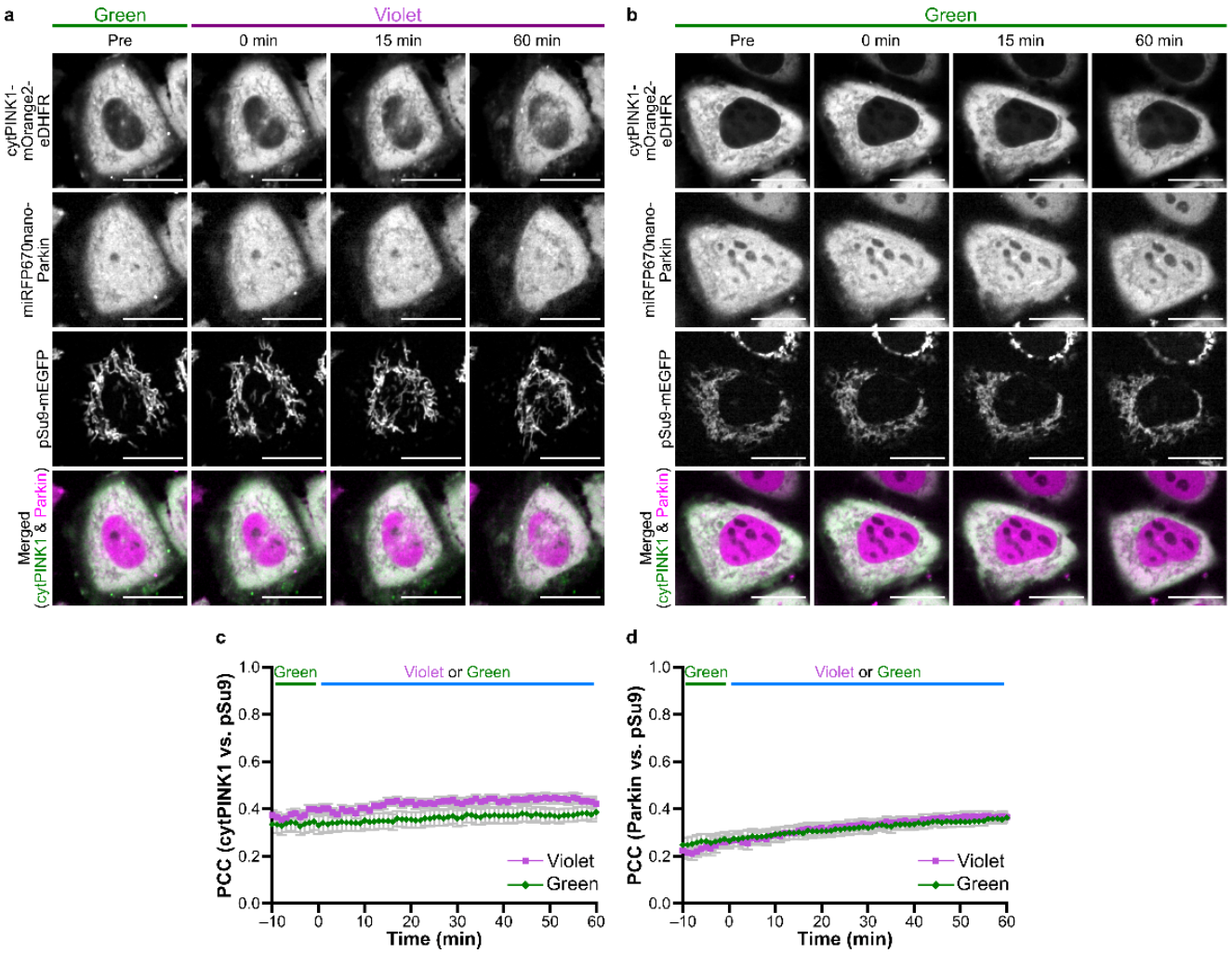

Extended Data Fig. 4 | Optical regulation of mitophagy without pcDH treatment. a,**b** Evaluation of mitophagy induced by light illumination. Confocal fluorescence images of HeLa cells expressing cytPINK1-mOrange2-eDHFR, miRFP670nano-Parkin, pSu9-mEGFP, and Halo-OMP25 without pcDH. Violet (405 nm) light was irradiated before the 0-min images were acquired and after every image acquisition (0–60 min, **a**). Green (555 nm) light was irradiated after every image acquisition to suppress the recruitment of cytPINK1-mOrange2-eDHFR by the excitation light (**b**). **c**,**d**, Time-course changes in PCC between cytPINK1-mOrange2-eDHFR and pSu9-mEGFP (**c**) or between miRFP670nano-Parkin and pSu9-mEGFP (**d**). The green line indicates green light illumination after every image acquisition, and the cyan line indicates violet or green light illumination after every image acquisition. Data are shown as the mean ± s.e.m., *n* = 15 cells, three independent experiments. Scale bars, 20 μm.

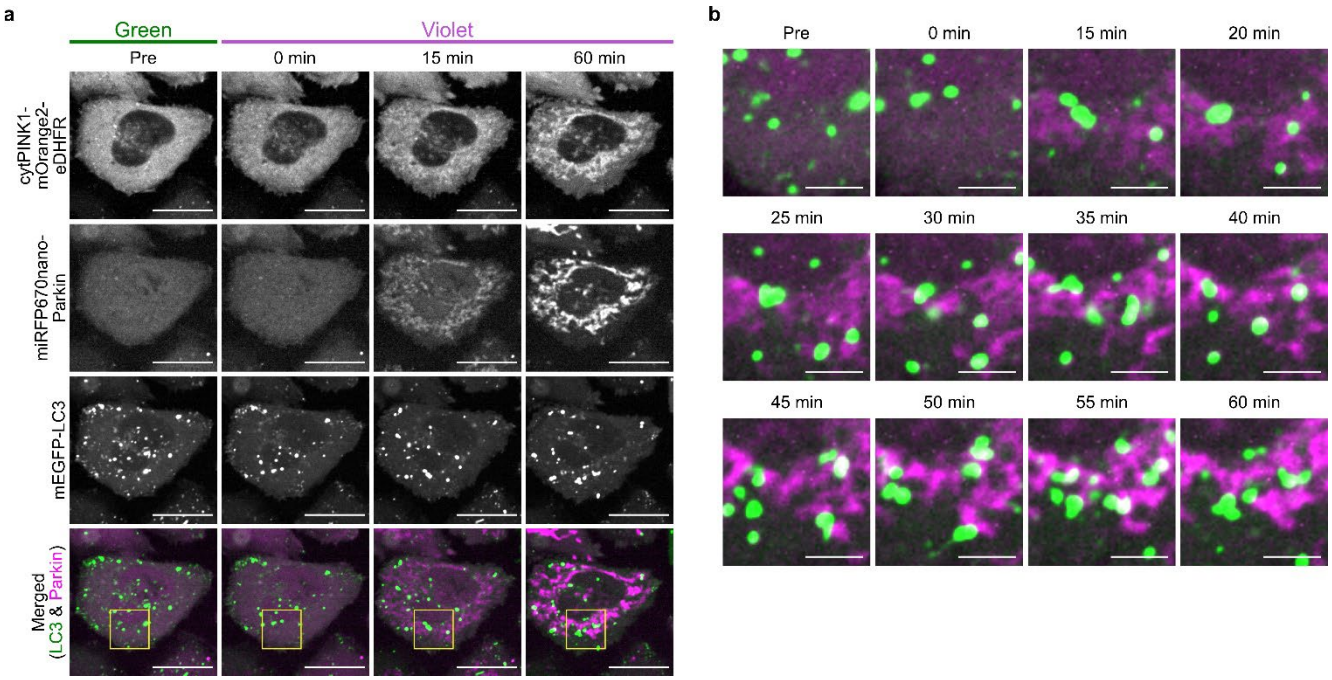

Extended Data Fig. 5 | Localization of the autophagy marker mEGFP-LC3 after induction of mitophagy by the photochromic CID system. a,**b** Confocal fluorescence images of HeLa cells expressing cytPINK1-mOrange2-eDHFR, miRFP670nano-Parkin, mEGFP-LC3, and Halo-OMP25, treated with 7 μM pcDH. Violet (405 nm) light was illuminated before the 0-min images were acquired and after every image acquisition (0–60 min). Enlarged images of the area indicated by the yellow squares in **a** (**b**). Scale bars, 20 μm (**a**) or 5 μm (**b**). Two independent experiments were performed.

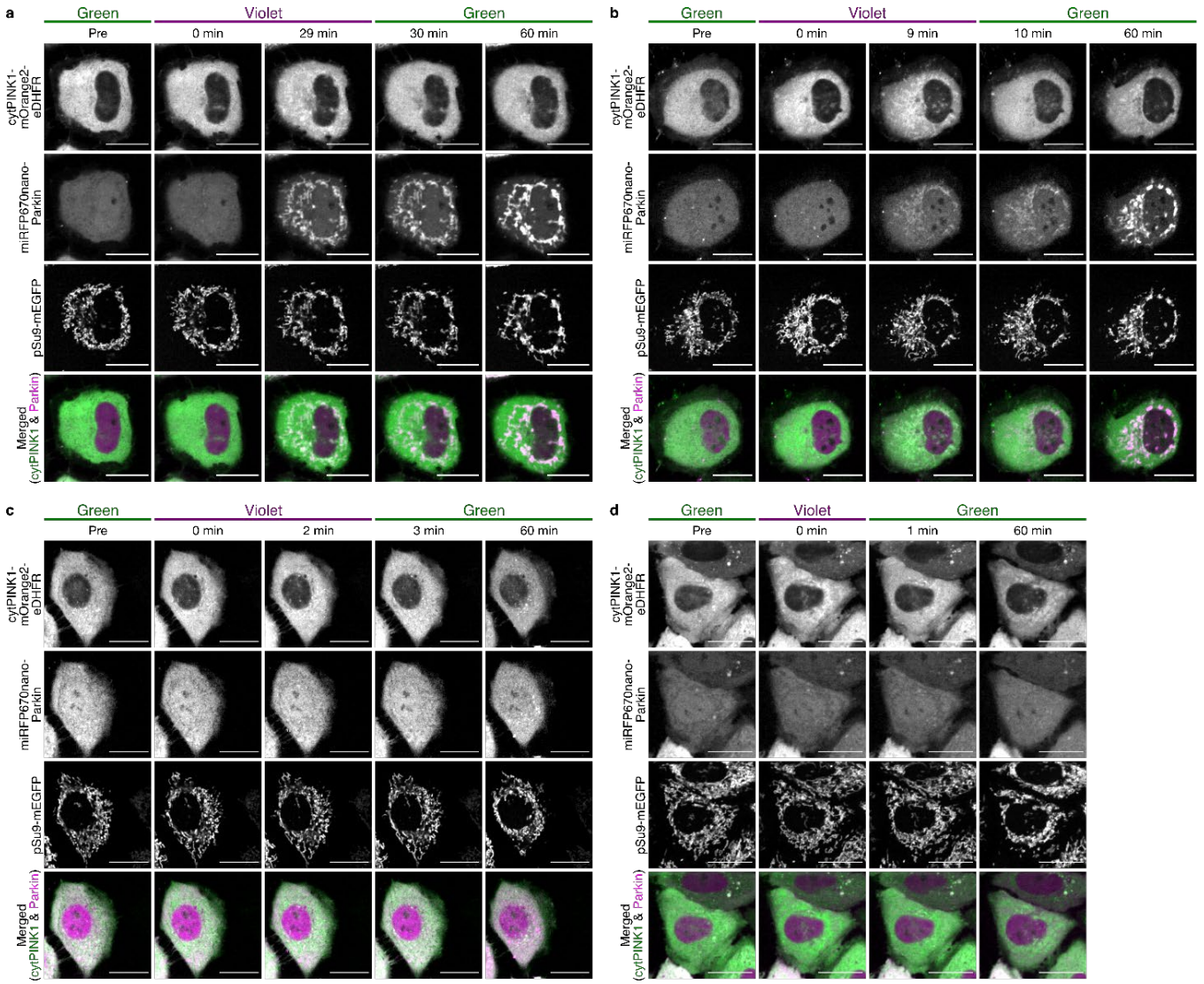

Extended Data Fig. 6 | Temporal recruitment of cytPINK1 to the MOM under alternating violet and green light illumination. Violet (405 nm) light was irradiated before the 0-min image acquisition and after every image acquisition during 0–29 min (**a**), 0–9 min (**b**), 0–2 min (**c**), or 0 min (**d**). Green (555 nm) light was irradiated before the 30-min (**a**), 10-min (**b**), 3-min (**d**), or 1-min (**d**) image acquisition and after every image acquisition (30–60 min, **a**; 10–60 min, **b**; 3–60 min, **c**; 1–60 min, **d**). Scale bars, 20 μm.